A Ground Penetrating Radar Lunar Analogue Field Campaign in the Haughton Impact Structure, Canada

T. Unrau, K.F. Tiampo, R.G. Pratt, G. Osinski
University of Western Ontario
Correspond via troy.unrau@gmail.com

Introduction

Ground-Penetrating Radar (GPR) has been widely cited as an important scientific instrument for future Moon and Mars surface exploration missions [Annan, 2002]. In support of GPR technique testing for lunar subsurface exploration, a series of overlapping 2D and 3D GPR surveys were conducted over impact melt rocks at the Haughton impact structure, Devon Island, Canada (Figure 1). This complex crater is estimated to be 39 Ma and 23 km in diameter [Lee and Osinski, 2005].

Figure 1 (above): Haughton Crater, Devon Island, Nunavut. 75° 22' N, 89° 41' W

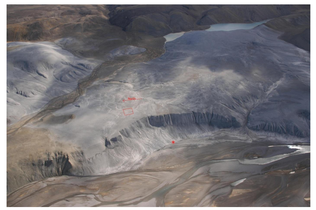

Figure 2 (above): Air photo of survey location. The grey unit is target of the survey, a calcite-dominated clast-rich melt rock. Survey location is marked in the red square. The site was selected to minimise the effect of major structural features nearby, such as frost wedges and polygonal terrain.

The target consisted of calcite-dominated clast-rich impact melt rock [Lee and Osinski, 2005] with permafrost at depths measured onsite at less than one metre. The target rocks were chosen as a physical analogue to lunar electrical conditions: the electrical permittivity of ice (K=3.2) and calcite (K=8-9) produces a better match for lunar electrical conditions (K=3-10) than liquid water (K =81) bearing analogue sites [Reynolds, 1997; Chung et al, 1970; Heiken et al., 1991].

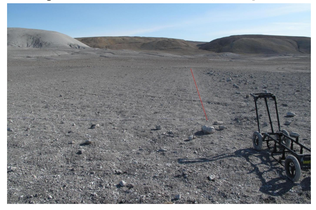

Figure 3 (above): Survey location looking East along the baseline (Y=0m).

GPR surveys were carried out using a PulseEkko Pro GPR system from Sensors and Software. This unit was equipped with interchangeable 200, 100 and 50 MHz antennas, a cart with odometer, and a PulseEkko IV 400V transmitter. The primary objective was to observe the effect of scattering on effective depth of signal penetration as a predictor for lunar response.

Velocity Measurement

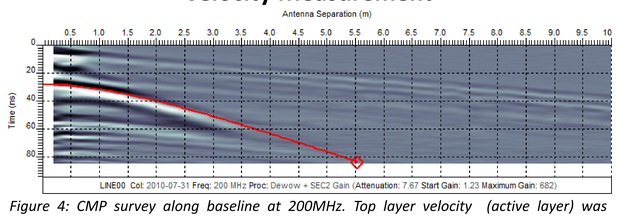

Figure 4: CMP survey along baseline at 200MHz. Top layer velocity (active layer) was matched with the hyperbola shown to be 0.070 m/ns.

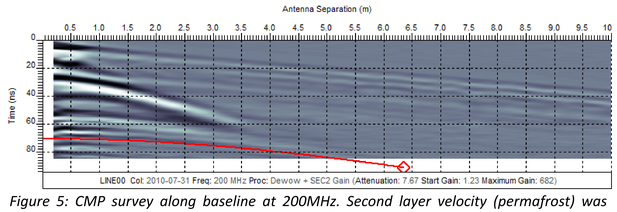

Figure 5: CMP survey along baseline at 200MHz. Second layer velocity (permafrost) was matched with the hyperbola shown to be 0.110m/ns.

2D Surveys

2D surveys were conducted at 200, 100 and 50 MHz on the baseline to provide an estimate for noise and 2D depth of penetration. These lines are presented in sequence in Figures 6.

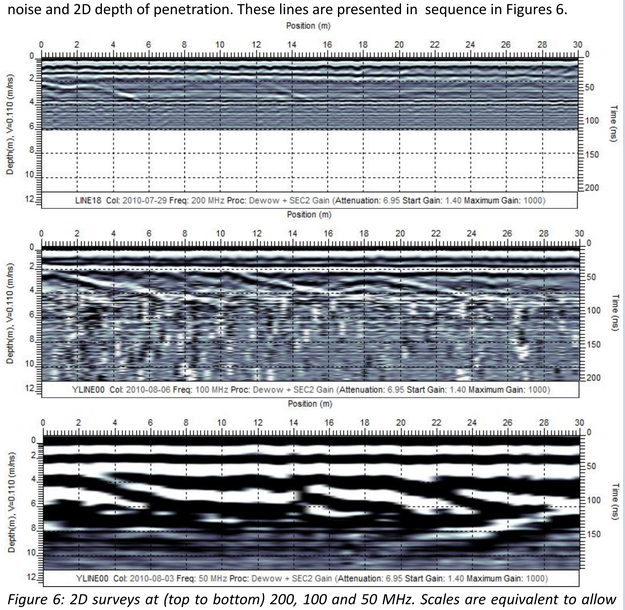

Figure 6: 2D surveys at (top to bottom) 200, 100 and 50 MHz. Scales are equivalent to allow for comparison between different frequencies. Depth estimate is assuming single layer at 0.110 m/ns and does not take into account a ~1 m slow layer (0.070 m/ns), which skews depths downwards by an estimated half a metre. Station spacings are 10, 25 and 50 cm respectively. Stacking via DynaQ.

Additional 2D surveys were performed to compare the response of the target area to those of the nearby intact dolomotic limestone. These surveys were performed at 100 MHz only and are presented for 400 m heading directly North from the grid origin (perpendicular to the baseline). As seen in Figure 7 and 8 , the signal response from depth becomes increasingly coherent as the survey transitions onto the dolomitic limestone megablock.

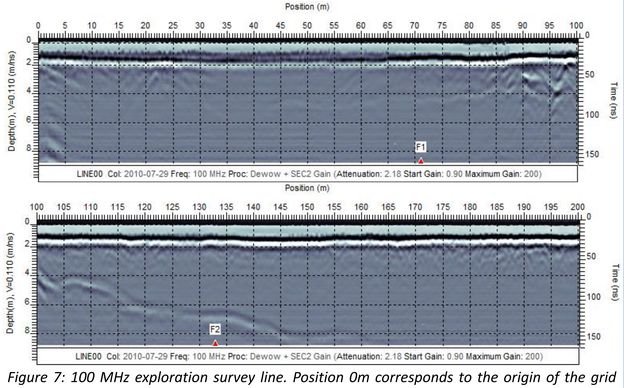

Figure 7: 100 MHz exploration survey line. Position 0m corresponds to the origin of the grid and baseline. The first 30m correspond to line X=0m. The line then procedes directly North (as indicated in Figure 1).

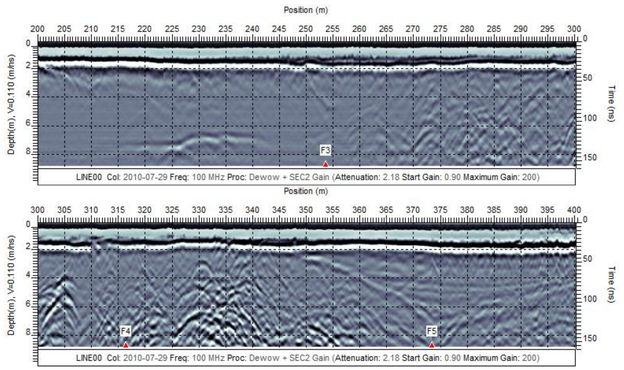

Figure 8: 100 MHz exploration survey line, continued. The transition to the next unit occurs at around 270 m at the surface. The character of this unit is quite different than the impact melt breccia unit, with coherence hyperbola and interfaces visible.

3D Surveys

The main survey at this location was a multifrequency 3D survey over a 30x30m grid. The baseline for this grid is the same as the CMP and 2D baseline surveys. The grids for the various frequencies are shown in Figure 9; survey parameters in Table 1. Example depth slices are plotted in Figure 10 and several depths slices for 100 MHz are plotted in Figure 11 to show its effectiveness. These slices have been filtered using the EkkoMapper default parameters.

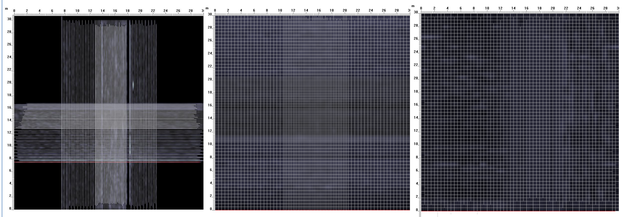

Figure 9 (above): Grid layouts for 3D surveys, after muted lines. From left to right: For 200 MHz, line spacing is 10 -25 cm; for 100 MHz, 25-50 cm; for 50 MHz, 50 cm.

Table 1 (below): Survey parameters for 3D. Where line spacing varies, it is due to tighter spacing in the centres of the grids.

Peak Frequency	Antenna Separation	Station Spacing	Line Spacing	Total Lines
200 MHz	50 cm	10 cm	10-25 cm	182
100 MHz	1 m	25 cm	25-50 cm	162
50 MHz	1 m	50 cm	50 cm	122

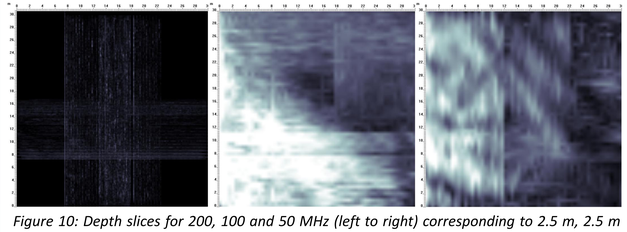

Figure 10: Depth slices for 200, 100 and 50 MHz (left to right) corresponding to 2.5 m, 2.5 m and 5.0 metres. The 200 MHz slice shows some subtle features on the left side while the same slice at 100 MHz shows the larger dichotomy running diagonally across the survey area. The 50 MHz slice shows several linear features that could be fractures.

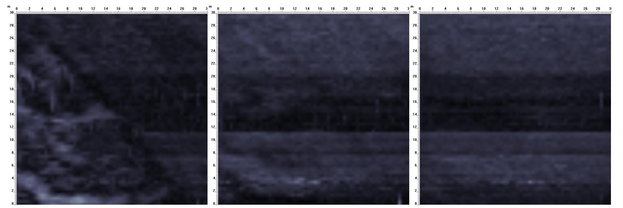

Figure 11: 100 MHz depth slices corresponding to 5.0, 5.5 and 6.0 m. There is a planar feature in this data that can be followed until it disappears at roughly 6.0 m. There is no clear evidence of this feature at depths beyond 5 m in the 2D surveys.

Analysis

The 2D plots show continuous interfaces that vanish at 2.5, 5 and 9 metres for 200, 100 and 50 MHz plots, respectively. When comparing the 4 m penetration for 100 MHz in the target lithology to the >8 m penetration in the neighbouring unit, the effect of the brecciation on the signal propagation becomes apparent.

The 3D plots show that faults can be traced to depths greater than what is visually apparent on the 2D plots. Depth of resolution in 3D is increased slightly to 3.0, 6 and 10 metres. While this suggests the usefulness of 3D imaging in improving depth resolution in a scattering medium, it is still less (at 100 MHz) than the 2D penetration in the neighbouring unit.

Additional analysis yet to be completed include: measuring the electrical conductivity and electrical permittivity in samples with varying water content and temperature. These values will be used to create a model for use in 3D GPR simulation to attempt to confirm the hypothesis that the scattering material is acting as an additional source of attenuation.

Conclusion

Physical analogue testing at the Haughton Crater suggests that signal scattering in brecciated materials significantly attenuates GPR. As a consequence, the depth of GPR usefulness for lunar exploration may be reduced in areas of highly brecciated material. The addition of 3D GPR data can help to improve the effective depth of penetration by approximately 20% in visual plots, however this requires significant additional data collection.

Additionally, performing these analogue tests in an environment that is electrically similar to the lunar surface help to confirm that the reflections seen are not simply strong reflectors from a water filled fracture or similar interface.

References

Annan, A. P. (2002), GPR—History, trends, and future developments, *Subsurface Sensing Technologies and Applications*, *3*(4), 253–270, doi:10.1023/A:1020657129590.

Chung, D. H., W. B. Westphal, and G. Simmons (1970), Dielectric Properties of Apollo 11 Lunar Samples and Their Comparison with Earth Materials, *J. Geophys. Res.*, *75*(32), PAGES 6524–6531.

Heiken, G., D. Vaniman, and B. M. French (1991), Lunar sourcebook: a user's guide to the moon, CUP Archive.

Lee, P., and G. R. Osinski (2005), The Haughton-Mars Project: Overview of science investigations at the Haughton impact structure and surrounding terrains, and relevance to planetary studies, *Meteoritics & Planetary Science*, *40*(12), 1755–1758.

Reynolds, J.M. (1997), An introduction to applied and environmental geophysics, John Wiley and Sons, Chichester.